Int. J. Electrochem. Sci., 12 **(2017)** 2987 – 3000, doi: 10.20964/2017.04.63

International Journal of ELECTROCHEMICAL SCIENCE
www.electrochemsci.org

Corrosion Study of Electroless Deposited Nickel-Phosphorus Solar Absorber Coatings on Carbon Steel

A. Sosa Domínguez[1,2], *J. J. Pérez Bueno*[1,*] , *I. Zamudio Torres*[1], *M. L. Mendoza López*[3]

[1] Centro de Investigación y Desarrollo Tecnológico en Electroquímica, S.C.; Parque Tecnológico Querétaro-Sanfandila, Pedro Escobedo, Qro. México. C.P. 76703; Tel.: (52-442) 2 11 6000; Fax: (52-442) 2 11 6001.
[2] Universidad Autónoma de Querétaro. Facultad de Química, Centro Universitario Cerro de las Campanas, C.P. 76010, Querétaro, Qro, México. E-mail: adrian.sosa@uaq.mx
[3] Tecnológico Nacional de México, Instituto Tecnológico de Querétaro, Av. Tecnológico s/n Esq. Mariano Escobedo, Col. Centro, Qro. México, C. P. 76000, Querétaro, México.
[*]E-mail: jperez@cideteq.mx

Received: 20 January 2017 / *Accepted:* 6 March 2017 / *Published:* 12 March 2017

One of the big challenges to sustainability is the solar energy conversion efficiency, and particularly in the case of conversion to thermal energy, is the absorbent surface, which has a leading role. In this work, coatings for solar-to-thermal energy conversion have been deposited onto carbon steel substrates from a nickel sulfate electroless bath, as a source of nickel and sodium hypophosphite as a reducing agent. Electroless black nickel surfaces were obtained, through etching of electroless nickel-phosphorous deposits with an oxidizing acid solution. EDX studies suggested that the coatings were constituted by 11% phosphorous. Surfaces predominantly covered by NiO were identified through XPS. By observing those problems that bring corrosion to metal surfaces, this work aims to determine the corrosion mechanism that degrades the surfaces of black nickel, and consequently, brings about the deterioration of their absorbent properties. Corrosion resistances of black electroless nickel-phosphorus coatings were investigated by polarization measurements, electrochemical impedance spectroscopy (EIS), electrochemical frequency modulation (EFM) and electrochemical noise in 0.5M NaCl solutions at room temperature and without stirring. The equivalent circuit for electrochemical impedance measurement, on the corrosion resistance of black electroless Ni-P deposits, consisted of the following elements: resistance of solution (R_s), the charge transfer resistance of the coating (R_{ct}) and a constant phase element. The EFM measurements were performed with 0.02 Hz and 0.05 Hz potential perturbation frequencies. The results of these studies show a decrease of corrosion resistance but associated with the increase of about four times the surface area of black coatings. The composition and roughness of each studied surface were directly associated with their corrosion rates.

Keywords: Electroless, Ni-P black, corrosion; steel; renewable energy.

1. INTRODUCTION

Surfaces with ultra-absorbent properties have been developed to take advantage of the energy from the sun, which can be prepared by different techniques such as physical vapor deposition, spray methods and electro-deposition [1,2]. A material with excellent solar absorption properties must have a high absorbance value and low emissivity [3-6].

Ni-P coatings have been deposited by the electroless technique from nickel (II) chloride baths containing hypophosphite on carbon steel substrates [1,7-12]. The hypophosphite is the reducing agent in the electroless nickel bath and its presence ensures the deposition of phosphorus [12-16]. The electroless Ni-P coatings are classified as: low phosphorus (1-4 wt.% P), medium phosphorus (5-9 wt.% P) and high phosphorus (above 10 wt.% P) [8-10,14,15].

Black absorbing coatings have a variety of applications and are used in daily life as decorative coatings and materials having absorbent capacities within the fields of aerospace and automotive [2,8,9,12,17-19]. They are obtained by oxidizing surfaces with an acidic solution [8,12]. Ultra high absorptance black coatings are of crucial importance in terrestrial and space-borne optical instruments. Also, they are useful as sensors for measurements in ultraviolet, visible and infrared spectral regions. These coatings are extremely useful to improve the absorptance of thermal detectors. They can reduce inner reflections or diffuse scattering in optical systems, such as microscope and telescope housing and some inner components [10,20].

In this work, Ni-P coatings were prepared and acid attacks on the surfaces were performed, obtaining black coatings of Ni-P with solar absorbing capacity in the region of the spectrum from 200 nm to 2500 nm. In order to determine the corrosion resistance of prepared coatings, electrochemical techniques were applied, such as: polarization curves, electrochemical impedance spectroscopy, electrochemical noise and electrochemical frequency modulation.

2. MATERIALS AND METHODS

The substrates used were AISI 1018 steel plates (C 0.15-0.2%; Mn 0.6-0.9%; P 0.04%; S 0.05%; Fe balance) with a surface finishing with sandpaper of a grain size of 600. The conditions used for the electroless nickel bath for the preparation of Ni-P coatings are shown in Table 1. To carry out the preparation of the black Ni-P coating, a superficial modification with full immersion in 9 mol L^{-1} nitric acid at room temperature and without stirring was performed for about 40 s, after rinse with distilled water. In this work, the following abbreviations are used: A) *steel + Ni-P coating*, which represents a steel substrate with a Ni-P layer; B) *steel + Ni-P coating + blackening*, which represents a steel substrate, a Ni-P coating and its etching to form a top black layer.

Corrosion of the coatings was evaluated using polarization curves, electrochemical impedance spectroscopy, electrochemical noise and electrochemical frequency modulation using a GAMRY potentiostat, model Reference 3000. An electrolyte of 0.5 mol L^{-1} NaCl was used for the application of electrochemical techniques. Electrochemical tests were performed for corrosion in a cell with graphite and saturated calomel electrodes as the counter electrode and the reference electrode, respectively.

Polarization curves were measured at a scan rate of 2 mV s^{-1} starting from -0.5 V to +0.5 V with respect to OCP. An AC voltage (sine wave) with an amplitude of 10 mV was used as the imposing signal, and the measurement frequency range was set from 1 MHz to 10 mHz. The following conditions were used in the electrochemical noise technique: block time of 1 s, a sample period of 0.01 s, repeat time of 0.05 min, and a total time of 0.25 h. EFM measurements were performed applying a potential perturbation signal with an amplitude of 10 mV with two sine waves of 2 and 5 Hz with a frequency base of 0.1 Hz, a DC voltage of 0 V *vs.* E_{OCP} and 4 cycles.

Table 1. Bath compositions and operating conditions of electroless Ni-P depositions.

Bath constituents and parameters	**Quantity (g L^{-1})**
Nickel sulfate ($NiSO_4$ $6H_2O$)	30
Sodium hypophosphite (NaH_2PO_2)	10
Sodium Citrate ($Na_3C_6H_5O_7$ $2H_2O$)	12.5
Sodium acetate (CH_3COONa)	5
Thiourea (NH_2CSNH_2)	0.001
Operating conditions	
pH	4.5 - 5.0
Temperature	88 - 90 °C
Time	3 hours

SEM images were obtained using a JEOL microscope, model JSM-6510LV with variable pressure, and in all the cases using 10 kV. The gray scale images were taken at 1900X with a scale bar of 10μm, and the area of the rectangle within the image corresponds to 2000X.

Profilometry was analyzed with a 3D optic microscope Bruker, model Contour GT. The image analysis was done using Gwyddion 2.44 software.

X-ray Photoelectron Spectroscopy (XPS) was analyzed with a Thermo Scientific K-Alpha, Al Kα photon energy hν = 1,486.6 eV. O1s peak position at 531.0 eV was used as an internal standard, instead of C1s, to detect and compensate the charge shift of the core level peaks. The preceding was conducted that way because C was not the main component of the surfaces. Ni2p core level spectrum was fitted using a Gaussian-Lorentzian mix function and Shirley type background subtraction. Throughout all measurements, the basic pressure in the analysis chamber was 10^{-9} mbar. Survey and high resolution core level spectra were collected at energy intervals of 1 eV and 0.1 eV, respectively. An X-ray beam, with 400 μm in spot size was employed to analyze three different regions located onto the sample surfaces.

An ocean optic USB2000 spectrometer with an integrating sphere was used for UV-visible region. The spectra in the MIR/NIR region was measured using a Perkin Elmer FTIR spectrometer (Frontier MIR/NIR) with an integrating sphere from 2 to 15 mm.

3. RESULTS AND DISCUSSION

Fig. 1a shows a SEM image of a Ni-P surface, obtained through the electroless technique where a surface with low roughness and high homogeneity is observed, which shows a similar morphology than other reports [21]. The lines observed in the image are attributed to the substrate surface finishing.

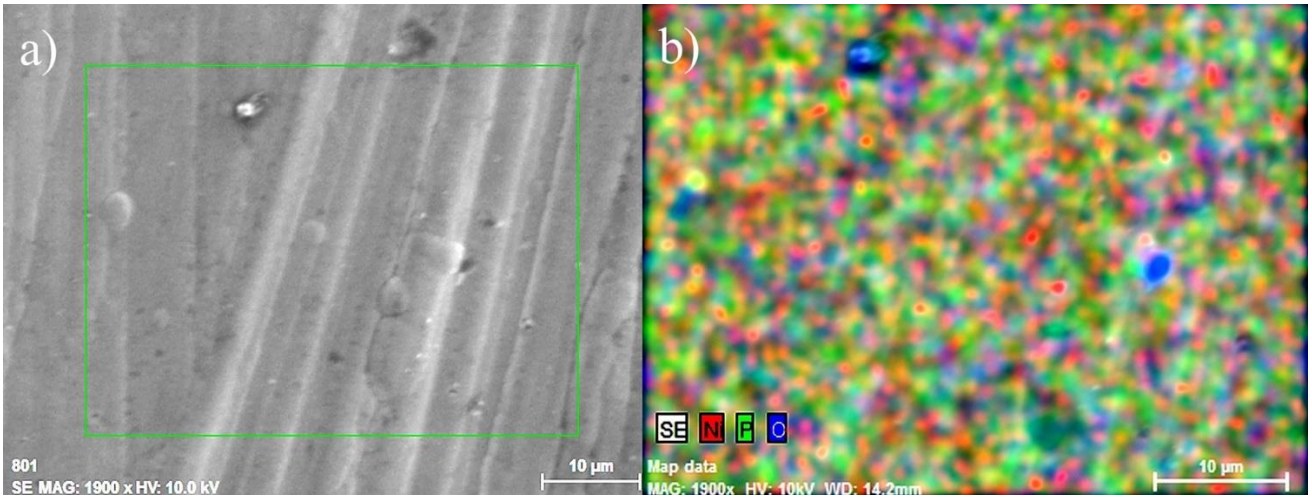

Figure 1. (a) Morphology by SEM of a Ni-P coating, and (b) EDX elemental mapping of a Ni-P coating.

Fig. 1b shows an EDX mapping image of the distribution of the elements Ni, P and O, which intersperse gray tones associated with the topography and the area corresponds to the rectangle of Fig. 1a. A random distribution of elements in the Ni-P coating is observed, but in different locations, some of the elements dominate. This means that in the nickel layer a regular distribution of phosphorus can be found. This condition is required for the blackening stage of the acidic attack. EDX analysis indicated the presence of phosphorus on the surface is about 11.3 wt.%, which as explained above, classifies the prepared samples as high phosphorus [8].

Fig. 2a shows a SEM image of a black Ni-P coating, where topographically elevated areas 5-10 µm in size were identified, separated by cracks of about 3 µm. The formation and dimensions of the elevated areas and cracks can be attributed to a dissolution process due to the acidic treatment, which was done to generate a black surface finish.

In Fig. 2b an EDX mapping image of the distribution of the elements Ni, P, O and C is observed. Gray tones are interspersed associated with the topography, and the area corresponds to the rectangle of Fig. 2a. Topographically, two main areas are observed: the raised areas and the cracks that separate them. The distribution of elements composing the coating is not uniform but rather preferential. Fig. 2c-2f individually show each of the elements in Fig. 2b; Ni, P, C, and O, respectively. The distribution of Ni is observed in Fig. 2c, and is more abundant primarily in cracks, which separate the raised areas of the coating. Fig. 2c shows a uniform distribution of phosphorus over the entire surface, without distinguishing between cracks and elevations. In Fig. 2e and 2f, the presence of C and O were observed mainly in the higher areas of the coating and inversely to that shown in Fig. 2c.

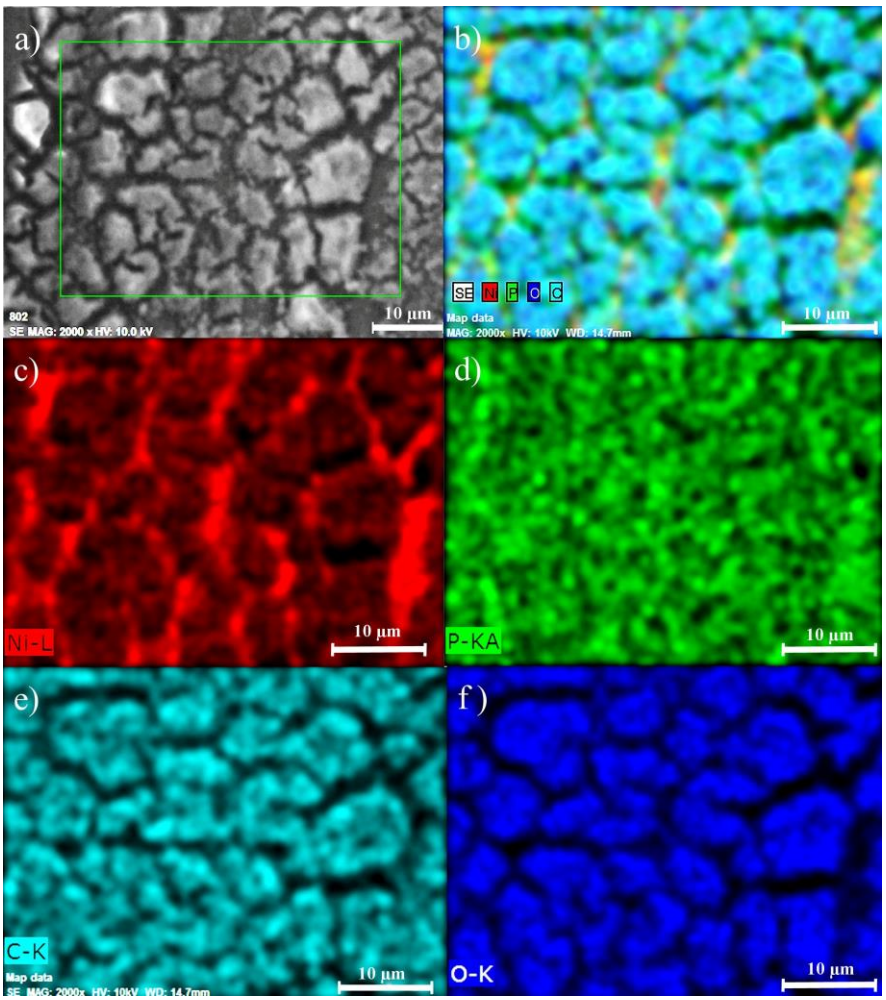

Figure 2. (a) Morphology by SEM of a black Ni-P coating, and EDX elemental mapping of a black Ni-P coating corresponding to: (b) multi-element image, (c) map of Ni, (d) map of P, (e) map of C, and (f) map of O.

According to the information observed in the EDX mapping of chemical composition, it can be proposed that the elevated areas are formed by nickel oxide accompanied by carbon. While the cracks have a higher proportion of nickel with a low degree of oxidation. With such compositions at the surface, it features a black hue with a high optical absorption capacity.

In Fig. 3, optical profilometry for Ni-P coating and black Ni-P coating on AISI 1018 steel are observed, with roughness values of 0.7 µm and 4.7 µm, respectively. This indicates that the surface with acid etching has a higher relief of the topography, which is directly associated with its characteristic optical absorption and, therefore, with their black color. In the case of Fig. 3a, the projected area (geometric area or area of a flat surface) was 75.2e-9 m^2 and 84.8e-9 m^2 of surface area. In the case of Fig. 3b, the projected area was 75.2e-9 m^2 and 320.2e-9 m^2 of surface area. This indicates a ratio of 1: 4.3 times the projected area, and increased by 2.8 times the surface area caused by the blackening process. This increase in area is directly proportional to the increase in the values of the i_{corr} and corrosion rate parameters.

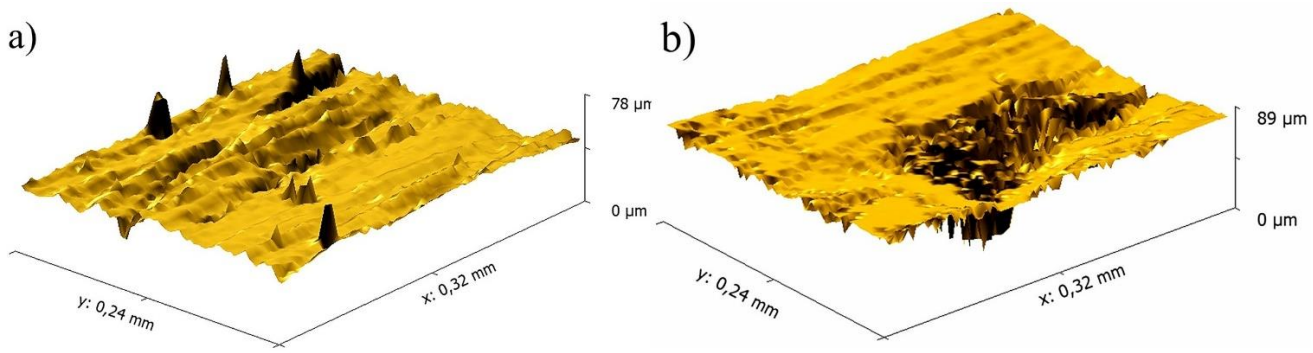

Figure 3. Optical profilometry for: (a) Ni-P coating, and (b) black Ni-P coating

The chemical bonding state of the films was analyzed by XPS. The Ni 2p contains Ni^{2+} as the main oxidation state, which is associated with NiO as constituting the top layer. The Fig. 4 provides the XPS spectra of Ni 2p core level spectrum, which consists of two sublevels $2p_{1/2}$ and $2p_{3/2}$. It can be noted that the binding energy of Ni $2p_{3/2}$ located at 853.2 eV, 856.2 eV, and 861.3 eV, corresponding to the first, second and third NiO peaks, respectively [22]. At the higher binding energy region of the spectrum, the peaks correspond to Ni^{2+} 2 $p_{1/2}$ and Ni^{3+} $2p_{1/2}$ peaks, respectively [23,24].

The splitting of Ni $2p_{3/2}$ spectrum is due to the presence of several oxidation states of Ni, including Ni^{2+} (NiO) and very low amount of Ni^{3+} (Ni_2O_3). Moreover, each oxidation state is accompanied by major and minor peaks, as well as satellite peaks. A binding energy of 853.2 eV corresponds to the Ni^{2+} $2p_{3/2}$ peak, which represents the feature of pure NiO.

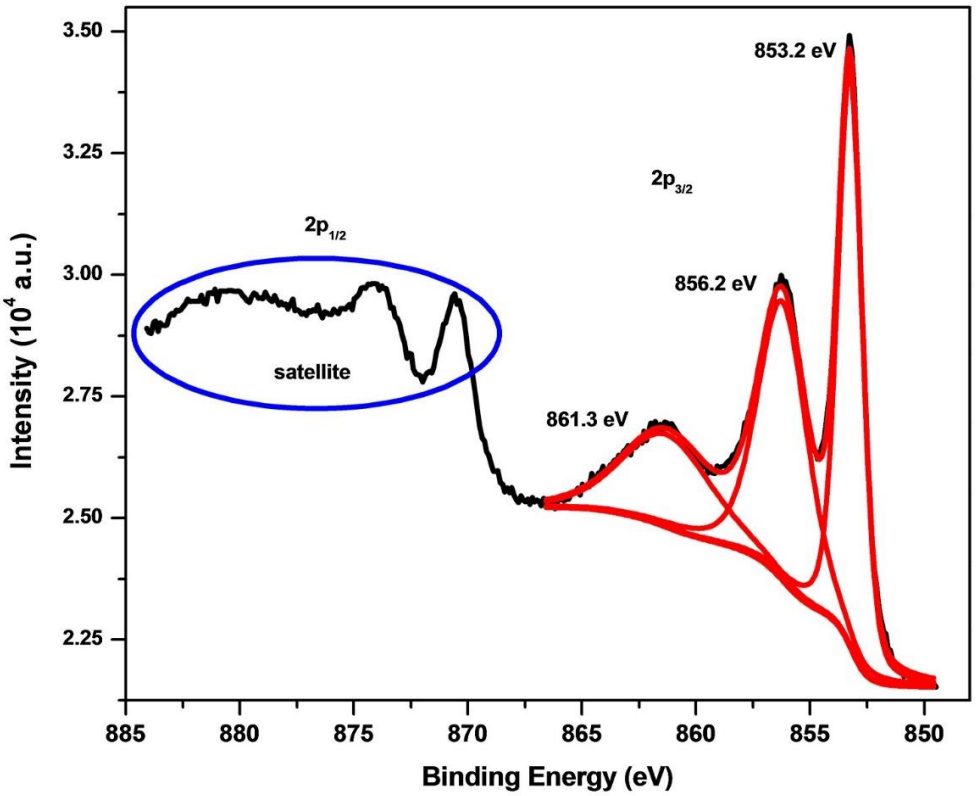

Figure 4. Ni 2p XPS core level spectrum showing the surface predominantly covered by NiO.

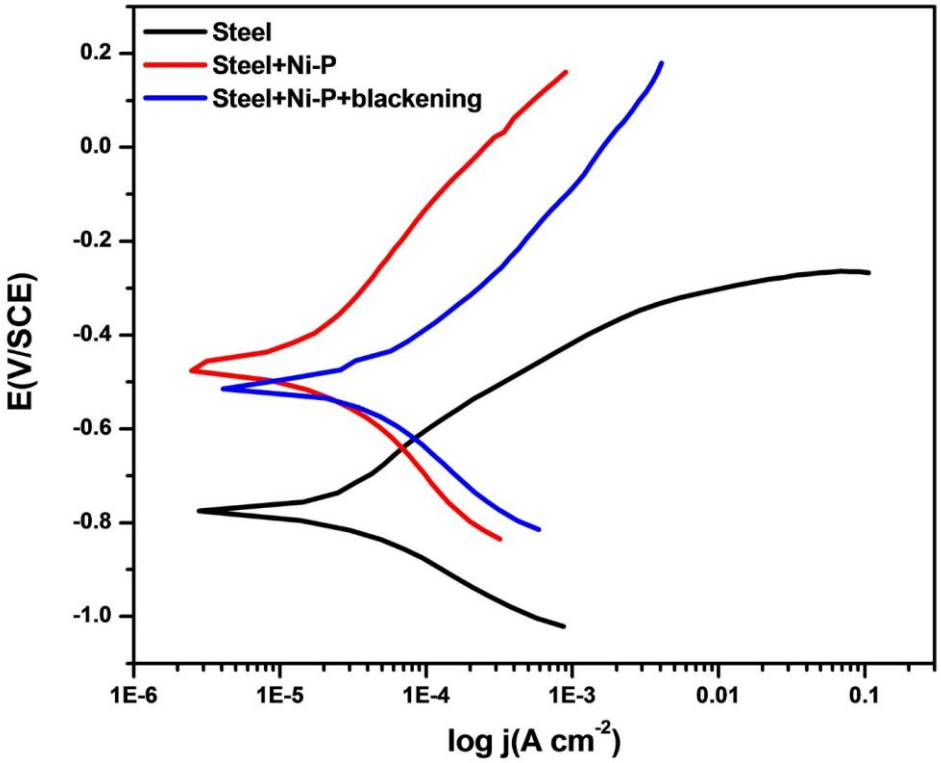

Figure 5. Polarization curves in 0.5 mol L^{-1} NaCl solution of AISI 1018 steel, *steel + Ni-P coating* and *steel + Ni-P coating + blackening*.

In Fig. 5, the polarization curve for the material used as the substrate is observed, with a potential corrosion value of -770 mV, and for *steel+Ni-P* coating and *steel+Ni-P coating+blackening* with values of corrosion potential of -454 mV and -511 mV, respectively [21]. The value of corrosion potential of the substrate is more negative than for the other two surfaces, which indicates that the surface was more susceptible to present a uniform corrosion. The values of corrosion current and polarization resistance of a surface Ni-P black, shown in Table 2, were 77.2 µA cm^{-2} and 2846 Ω cm^2. They are superior to those exhibited by steel but lower than *steel + Ni-P*. The R_p values from the Table 2 show that the surfaces *steel+Ni-P* and *steel+Ni-P+blackening* were resistant to corrosion with values above those of the bare substrate.

In Table 2 the corrosion potential, corrosion current, corrosion rate, and polarization resistance are observed from polarization curves of AISI 1018 steel, *steel + Ni-P coating* and *steel + Ni-P coating + blackening*. The values in Table 2 are consistent with the values given in the literature for steel [25]. The values of corrosion rate remained virtually unchanged for *steel + Ni-P* as they have a coating of *Ni-P + blackening* with values of 5.4 mm per year and 5.5 mm per year, respectively. This similarity results important considering that the latter had a NiO layer on top. In the case of steel, the surface tested has a value of 35.3 mm per year. This can be attributed to the time of carrying out the acid attack on the surface and the behavior of a Ni-P black coating on steel, which is less susceptible of being corroded than the bare steel.

Table 2. Corrosion potential and corrosion current in 0.5 mol L^{-1} NaCl solution obtained from the polarization curves.

	E_{corr} (mV)	i_{corr} (μA cm^{-2})	β_a (V/decade)	β_c (V/decade)	Corrosion rate (mm per year)	R_p (Ω cm^2)
Steel	-770	60.7	179e-3	127e-3	35.3	1139
Steel + Ni-P	-454	11.9	398e-3	295e-3	5.4	5466
Steel + Ni-P + blackening	-511	12	360e-3	380e-3	5.5	2846

The corrosion potential, E_{corr} of *steel + Ni-P + blackening* was more positive for uncoated steel. The corrosion current density, i_{corr} of *steel + Ni-P + blackening* decreased from 12 μA cm^{-2} with respect to the value of the steel which was 60.7 μA cm^{-2}. Of Table 2 it is also possible to observe that the polarization resistance, R_p was of de 2846 Ω cm^2 of *steel + Ni-P + blackening* which was twice the value of R_p obtained when there is no coating and the corrosion rate went from 35.3 mm/year to 5.5 mm/year increasing its resistance to corrosion. These results indicate that the application of a black Ni-P coating on an AISI 1018 carbon steel substrate improves the corrosion resistance properties in a 0.5 M NaCl solution.

In Fig. 6, Nyquist plots for AISI 1018 steel, Ni-P coating, and black Ni-P coating are observed. It can be seen that the loop size for the coating of Ni-P is larger than for the other two tested samples, which indicates that the Ni-P coating has a higher resistance to corrosion. The parameters obtained from Nyquist plots can be seen in Table 3. There were a relationship between the values of R_{ct} and those of R_p for the three surfaces as shown in Table 2 and Table 3. This confirms what has been said for the polarization curves and a proportional dependency to the increase in area between the surfaces.

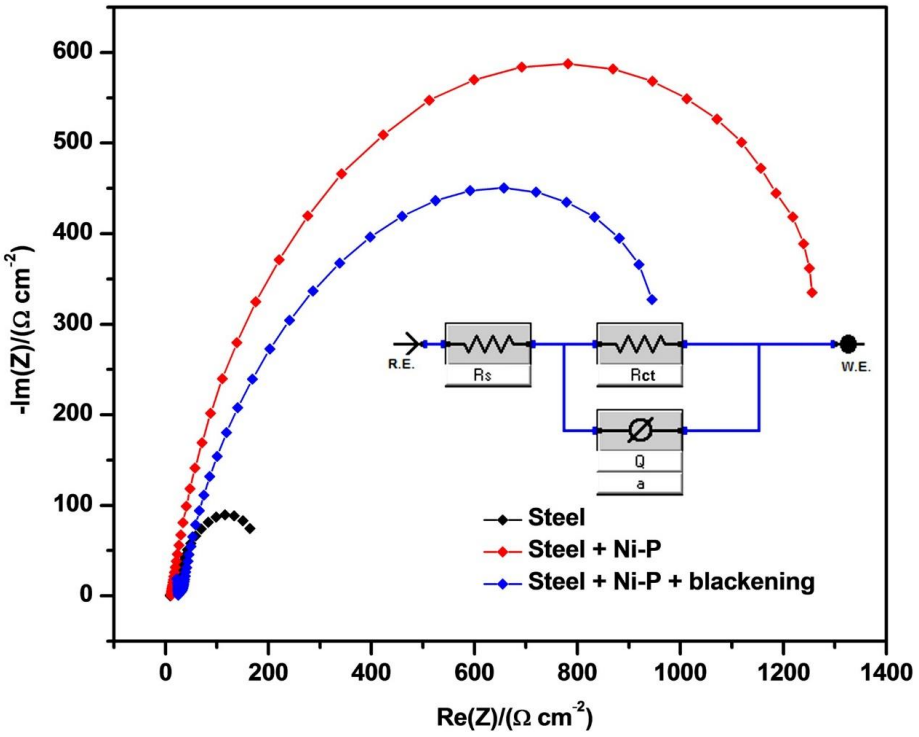

Figure 6. Nyquist plots for steel, *steel + Ni-P coating* and *steel + Ni-P coating + blackening* obtained in 0.5 mol L^{-1} NaCl solution. The insert shows their equivalent circuit.

In Table 3, the parameters obtained after making the settings by an equivalent circuit in Fig. 6, are shown. There, R_s is the solution resistance, R_{ct} is the charge transfer resistance of the coating, and Q is a constant phase element. Using the Simplex method [26], the resistance and capacitance values shown in Table 3 were obtained.

Table 3. Fitting of Nyquist plots on equivalent circuit described in Fig. 6.

	$R_s(\Omega\ cm^2)$	$R_{ct}(\Omega\ cm^2)$	Q ($S*s^a$)	a
Steel	10.1	283	4.5e-3	0.79
Steel + Ni-P	10.6	1.4e3	273e-6	0.82
Steel + Ni-P + blackening	10.3	1e3	7.6e-3	0.78

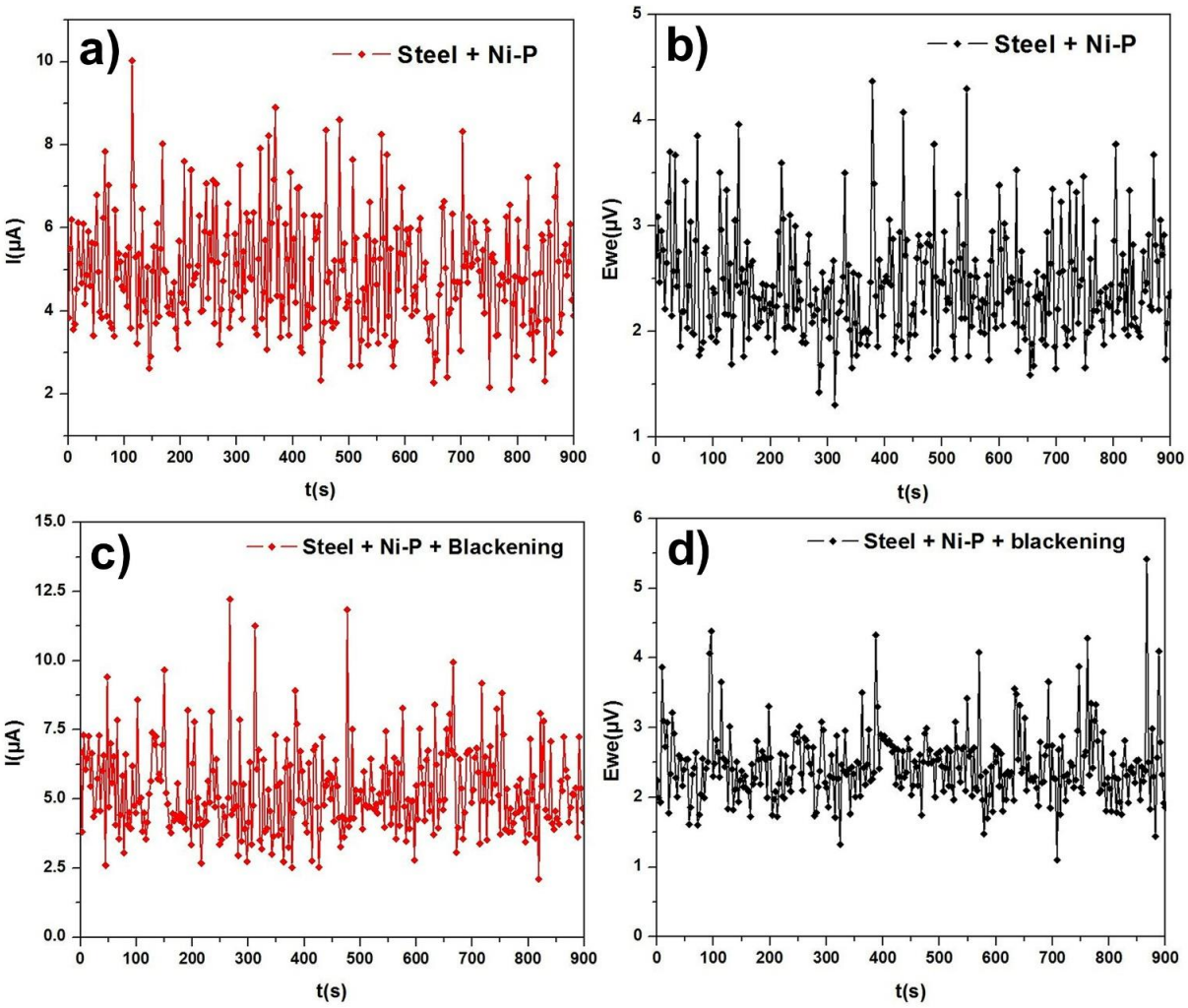

Figure 7. Potential noise and current noise for: (a) and (b) *steel + Ni-P coating*, (c) and (d) *steel + Ni-P coating + blackening*, respectively.

The resistance solution values, as seen in Table 3, remained constant around 10 Ω cm^2. For the values of corrosion resistance, it can be seen that the steel substrate had a value of 283 Ω cm^2, while for the Ni-P coating and black Ni-P coating were 1.4e3 Ω cm^2 and 1e3 Ω cm^2, respectively. This indicates that the Ni-P protects the surface from having a corrosion process. However, when it has a coating of Ni-P black the corrosion resistance of the surface decreases indicating less resistance of the coating to prevent the advance of corrosion but of similar magnitude. Cui *et al.* [9] conducted a corrosion study with 2.89 to 12.9 in the phosphorus content obtaining R_{ct} values in the range 1.356e3 Ω cm^2 to 5.772 e3 Ω cm^2, respectively. Considering some small differences in the experimental conditions, these results are in agreement with those in Table 3.

In Fig. 7 a difference in the amplitude of the oscillations in both, potential and current, due to the nature of the surfaces tested is observed. The electrochemical noise technique reflects the individual sum of random events and potential fluctuations in current, the steel substrate 1018 and coatings Ni-P and Ni-P black. The values of root mean square (RMS) of the amplitude of these events or standard deviation were 1.3 μA and 1.6 μA for the time series in current Fig. 7a and 7c, respectively. For the time series in potential, RMS values were obtained of 0.51μV and 0.52μV as shown in Fig. 7b and 7d, respectively. The fluctuations seen in Fig. 7 are linked to variations in the speed of the anodic and cathodic reactions, as a result of stochastic (breaking and re-passivation of the passive film) and deterministic processes (formation and propagation of pitting).

Abrupt current transients can be seen from the current time series in Fig. 7a and 7c, and can be associated with localized pitting nucleation sites. In both series of time of Fig. 7, both potential and current are observed for the anodic transients. It can be noticed, that in some cases, the current transients in Fig. 7a and 7c have high frequencies and very short durations at low intensities of the order of 4e-6 A cm^{-2}, which could be associated with the nucleation of the pitting.

Table 4. The parameters obtained from electrochemical noise measurements.

	I(μA)	**E(μV)**	**R_n (Ω cm^2)**	**I_L**	**Type of corrosion**
Steel	4.9	4.1	0.3	0.31	Pitting
Steel + Ni-P	4.9	2.4	0.4	0.28	Pitting
Steel + Ni-P + blackening	5.3	2.5	0.3	0.30	Pitting

In Table 4 the pitting index values around 0.3 are observed, which indicates that the corrosion present on the tested surfaces was of localized type.

In Fig. 8, current I *vs.* frequency f plots in 0.5 mol L^{-1} NaCl solution with b.f. = 0.1 Hz are observed for *steel + Ni-P coating*, and *steel + Ni-P coating + blackening*.

In Table 5 the results for corrosion current and corrosion rate for different surfaces tested are shown. It appears that the corrosion rate for carbon steel substrate is 7.8e3 mm per year and 86.9 mm per year for the black Ni-P coating, which indicates that black coating Ni-P is less susceptible to present a corrosive process, increasing the protection property for the substrate. In Table 5 causality factors CF(2) and CF(3) are observed, with theoretical values very close to 2 and 3, which leads us to consider valid measurements in electrochemical frequency modulation technique.

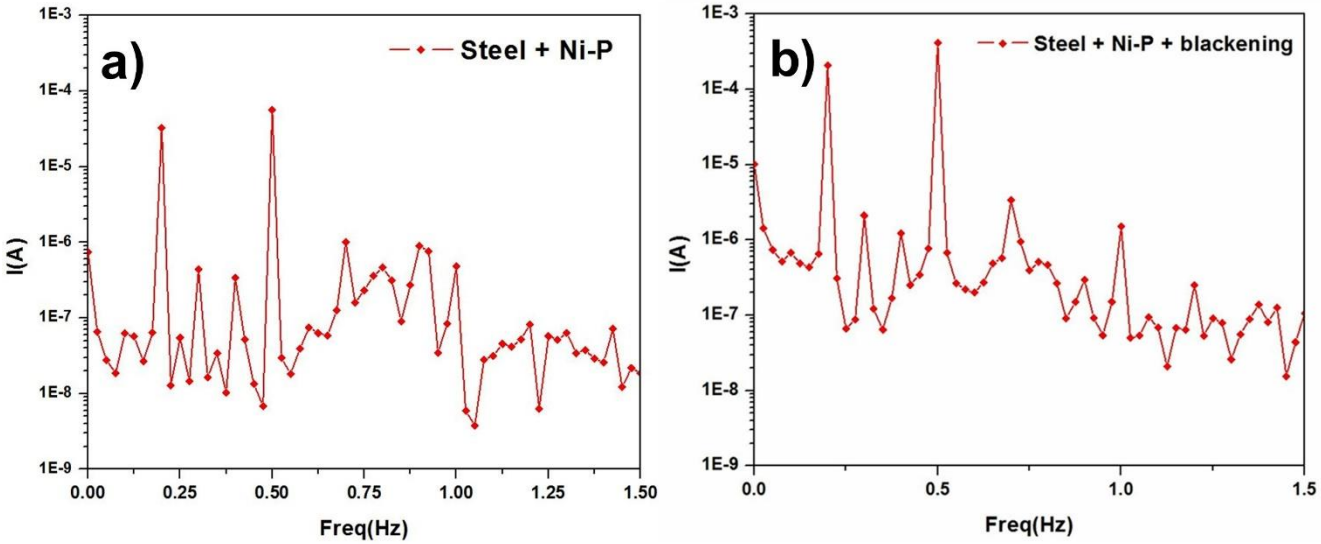

Figure 8. Current I *vs.* frequency plots in 0.5 mol L^{-1} NaCl solution with b.f. = 0.1 Hz: (a) *steel + Ni-P coating*, and (b) *steel + Ni-P coating + blackening*.

Table 5. Electrochemical parameters obtained with EFM technique.

	i_{corr}(μA cm^{-2})	Corrosion rate (mm per year)	CF(2)	CF(3)
Steel	190.1	7.8e3	2.0	3.0
Steel + Ni-P	0.15	80.6	1.8	2.9
Steel + Ni-P + blackening	0.17	86.9	2.0	2.8

Table 6. Polarization resistance in 0.5 mol L^{-1} NaCl solution determined with EFM technique.

	i_{corr} (μA cm^{-2})	B(V/decade)	R_p(Ω cm^2)
Steel	190.1	0.031	106
Steel + Ni-P	0.15	1.902	711
Steel + Ni-P + blackening	0.17	1.816	625

The values of the corrosion current are shown in Table 6. The B (Tafel constant) value and the R_p value were obtained by the technique of electrochemical frequency modulation. Also, Table 3

shows the values of R_{ct} obtained by the technique of electrochemical impedance spectroscopy and it is observed that the values are similar, which is a good indication of the scope of both techniques to reliably explain the phenomenon of corrosion that could present different surfaces such as AISI 1018 carbon steel and Ni-P coatings.

Taking into account the differences between the four techniques and not looking for a direct comparison between the measured parameters, the overall perception is that the Ni-P black coating is less susceptible to have corrosion. In this regard, the oxide layer of nickel formed in the process of acid attack has the characteristic of a physical barrier that protects against corrosion because this layer has cracks, exposing areas of a lower degree of oxidation, revealed by the oxygen present.

Phosphorus, being the element that is directly associated with the process of blackening, was found regularly distributed on the surface before and after that process, with only a slight decrease in its percentage. This is directly related to the fact that the corrosion process in the material did not change the nature of its chemical constitution.

We have been conferring to the surfaces a property of optical absorption without changing the nature of the elements that may be affected by a corrosive process, except the amount of exposure of each area.

Fig. 9a-c show the total reflectance spectrum for *Steel + Ni-P + blackening*: a) visible – near-infrared (Vis-NIR) and b) Near-infrared – mid-infrared (NIR-MIR). In the case of Fig. 9a, the reflectance is near to zero, which indicates that the surface characteristic was of low reflectivity. In the case of Fig. 9b, which continues the previous region, there was a peak about 940 nm which gradually decreased, and continued at about 5% in reflectance. One of the desired characteristics for a surface devoted to sunlight absorption is a reflectance approaching zero. In the case of the spectrum shown in Fig. 9a and Fig. 9b, the values were close to zero [1,12].

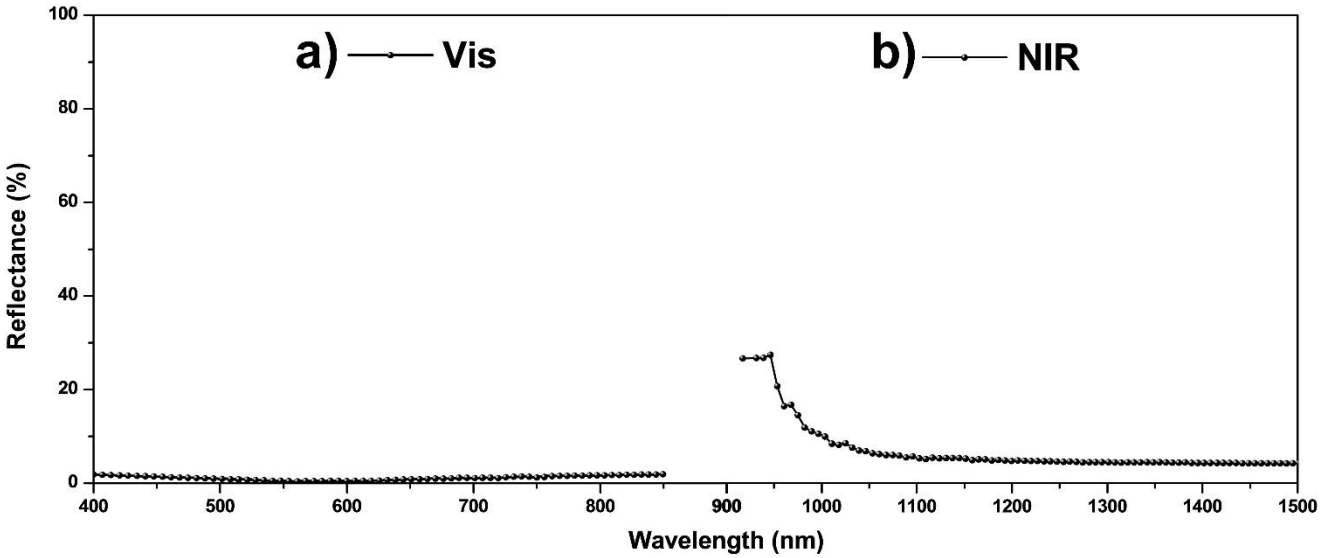

Figure 9. The total reflectance spectrum of sample *steel + Ni-P coating + blackening* in the electromagnetic spectrum regions: (a) Vis-NIR and (b) NIR-MIR.

Considering that the samples had not transmittance and that the measurement was taken at room conditions (without a strong infrared emission), the absorbance of the sample may be inverse to reflectance, and instead of appearing at the bottom of the graphs, it could be near the top of them.

It should be considered that the solar spectrum covers the range from about 200 nm up to about 2500 nm. Therefore, the samples under study fulfill such characteristics of low reflectivity and high absorption.

4. CONCLUSIONS

The purpose of this study was to perform a corrosion study of different surfaces that form part of the preparation of the black surface intended to be used for sunlight absorption, such as: AISI 1018 steel, *steel + Ni-P coating*, and *steel + Ni-P + blackening*. The above-mentioned study was conducted using electrochemical techniques such as polarization curves, electrochemical impedance spectroscopy, electrochemical noise and electrochemical frequency modulation. The steel *surface+Ni-P+blackening* has proven to have suitable optical properties, which makes it important to conduct a study of corrosion in order to understand the resistance of the coating to a corrosion process in 0.5 mol L^{-1} NaCl solution.

The SEM images show that morphology of the black Ni-P coating comprises significantly elevated areas and cracks with amounts of Ni and P featuring a high phosphorus coating. The XPS analysis showed that the surfaces were predominantly covered by NiO.

The black Ni-P coating showed a great capacity to corrosion protection with values of R_p 2,846 Ω cm^2, R_{ct} 1e3 Ω cm^2, R_n 0.3 Ω cm^2, and R_p obtained by the EFM technique of 625 Ω cm^2. Although these values are not directly comparable by the scope of each of the electrochemical techniques, all agree in showing low levels of corrosion resistance. Regarding the corrosion mechanism, it could be determined by the technique of EFM, which resulted in a localized corrosion type, indicating nucleation and formation of pitting on coatings tested in a 0.5 mol L^{-1} NaCl solution, under the conditions of application of the electrochemical techniques mentioned above.

ACKNOWLEDGEMENTS

The authors gratefully acknowledge the financial support from the Mexican Council for Science and Technology (CONACYT, Grants CEMIE-Sol No. 207450; QRO-2014-C03-250295; QRO-2012-C01 No. 191210). In addition, the first author acknowledges CONACYT for his graduate fellowship. Special thanks to Dr. Fabricio Espejel Ayala (CIDETEQ) for his invaluable help in obtaining the SEM images. Thanks to Curtiss Palin and Eric Albert Huston for their valuable comments about improving this written work.

References

1. F. I. Lizama-Tzec, J. D. Macías, M. A. Estrella-Gutiérrez, A. C. Cahue-López, O. Arés, R. de Coss, J. J. Alvarado-Gil, G. Oskam, *J Mater Sci: Mater Electron*, 26 (2014) 5553-5561.
2. J. M. Li, C. Cai, L. X. Song, J. F. Li, Z. Zhang, M. Z. Xue, Y. G. Liu, *Trans. Nonferrous Met. Soc. China*, 23 (2013) 2300-2306.

3. S. Zhao, E. Wäckelgard, *Solar Energy Materials & Solar Cells*, 90 (2006) 243-261.
4. F. Bensebaa, D. Di Domenicantonio, L. Scoles, D. Kingston, P. Mercier, G. Marshall, *International Journal of Low-Carbon Technologies*, 26 (2014) 1-5.
5. A. R. Shashikala, A. K. Sharma, D. R. Bhandari, *Solar Energy Materials & Solar Cells*, 91 (2007) 629-635.
6. A. R. Shashikala, R. Uma Rani, A. K. Sharma, S. M. Mayanna, *Galvanotechnik*, 97 (2006) 2387-2400.
7. R. Uma Rami, A. K. Sharma, C. Minu, G. Poornima, S. Tejaswi, *J Appl Electrochem*, 40 (2010) 333-339.
8. Y. Liu, D. Beckett, D. Hawthorne, *Applied Surface Science*, 257 (2011) 4486-4494.
9. G. Cui, N. Li, D. Li, J. Zheng, Q. Wu, *Surface & Coatings Technology*, 200 (2006) 6808-6814.
10. V. Saxena, R. U. Rani, A. K. Sharma, *Surface & Coatings Technology*, 201 (2006) 855-862.
11. L. Li, M. An, *Journal of Alloys and Compounds*, 461 (2008) 85-91.
12. R. J. C. Brown, P. J. Brewer, M. J. T. Milton, *J. Mater. Chem.*, 12 (2002) 2749-2754.
13. M. Palaniappa, G. V. Babu, K. Balasubramanian, *Materials Science and Engineering A*, 471 (2007) 165-168.
14. J. Sudagar, J. Lian, W. Sha, *Journal of Alloys and Compounds*, 571 (2013) 183-204.
15. Z. Qi, W. Lu, A. Guo, Y. Hu, W. Lee, *Ind. Eng. Chem. Res.*, 53 (2014) 3097-3104.
16. J. T. W. Jappes, B. Ramamoorthy, P. K. Nair, *Journal of Materials Processing Technology*, 169 (2005) 308-313.
17. F. He, H. Su, H. Ju, L. Tan, Q. Zhou, *Surface & Coatings Technology*, 213 (2012) 133-138.
18. O. R. M. Khalifa, E. Sakr, *The Open Corrosion Journal*, 2 (2009) 211-215.
19. E. Georgiza, J. Novakovic, P. Vassiliou, *Surface & Coatings Technology*, 232 (2013) 432-439.
20. V. Saxena, R. Uma Rani, A. K. Sharma, *Galvanotechnik*, 97 (2006) 827-840.
21. T. Rabizadeh, S.R. Allahkaram, A. Zarebidaki, *Materials and Design*, 31 (2010) 3174-3179.
22. K. Kaviyarasu, E. Manikandan, J. Kennedy, M. Jayachandran, R. Ladchumananandasiivam, U. Umbelino De Gomes, M. Maaza, *Ceramics International*, 42 (2016) 8385–8394.
23. K. Sajilal, A. Moses Ezhil Raj, *Materials Letters*, 164 (2016) 547-550.
24. Z. Qi, W. Lee, *Tribology International*, 43 (2010) 810-814.
25. F. Depenyou Jr., A. Doubla, S. Laminsi, D. Moussa, J. L. Brisset, J. M. Le Breton, *Corrosion Science*, 50 (2008) 1422-1432.
26. M. A. A. Kappel, R. Fabbri, R. P. Domingos, I. N. Bastos, *Measurement*, 94 (2016) 344–354.